Transition Path Times for Nucleic Acid Folding Determined from Energy-Landscape Analysis of Single-Molecule Trajectories

Krishna Neupane,[1] Dustin B. Ritchie,[1] Hao Yu,[1] Daniel A. N. Foster,[1] Feng Wang,[2] and Michael T. Woodside[1,2]

[1]*Department of Physics, University of Alberta, Edmonton, Alberta, T6G 2E1 Canada*

[2]*National Institute for Nanotechnology, National Research Council Canada, Edmonton, Alberta, T6G 2M9 Canada*

(Received 10 April 2012; published 6 August 2012)

The duration of structural transitions in biopolymers is only a fraction of the time spent searching diffusively over the configurational energy landscape. We found the transition time, τ_{TP}, and the diffusion constant, D, for DNA and RNA folding using energy landscapes obtained from single-molecule trajectories under tension in optical traps. DNA hairpins, RNA pseudoknots, and a riboswitch all had $\tau_{TP} \sim 10$ μs and $D \sim 10^{-13-14}$ m^2/s, despite widely differing unfolding rates. These results show how energy-landscape analysis can be harnessed to characterize brief but critical events during folding reactions.

DOI: 10.1103/PhysRevLett.109.068102 PACS numbers: 87.15.Cc, 05.20.Dd, 82.37.Np, 87.80.Cc

A quantitative, microscopic description of how biological macromolecules fold into complex three-dimensional structures remains one of the grand challenges of biophysics. Ensemble biochemical and biophysical measurements have provided significant insights into the folding problem [1], complemented in recent years by single-molecule approaches offering ever more detailed pictures of the microscopic behavior [2,3]. Such measurements, however, have invariably concentrated on characterizing stable or metastable states and their lifetimes, which range from milliseconds to minutes [1,4], rather than the paths taken between the states and the duration of the structural transitions. It is the transition paths which contain the key microscopic information about the folding reaction mechanisms, but the transitions themselves are extremely challenging to observe experimentally because they are very brief [5–7]. Until recently, only all-atom simulations could provide insight into the mechanistic details of the transition paths [8]. Advances in high-resolution single-molecule techniques, however, are now also enabling experimental characterization of transition paths.

Folding reactions are usually described in terms of diffusion over a configurational energy landscape, often reduced to a 1D profile along an appropriate reaction coordinate [9]. The reduction in entropy as the molecule is funneled towards the folded state competes with the enthalpy of intrachain interactions to produce a free-energy barrier for folding [Fig. 1(a)]. The folding or unfolding rate can then be determined from the free-energy profile by Kramers theory [10]:

$$k = k_0 \exp\left(-\frac{\Delta G^{\ddagger}}{k_B T}\right), \qquad \text{where } k_0 = \frac{\sqrt{\kappa_w \kappa_b}}{2\pi k_B T} D, \quad (1)$$

$\Delta G^{\ddagger}$ is the energy barrier height (which dominates the kinetics), D is the diffusion constant for barrier crossing, κ_w is the stiffness (curvature) of the potential well, and κ_b is the stiffness of the barrier. Most of the time spent between folding or unfolding transitions ($\tau = 1/k$), however, merely involves diffusion within the potential wells; the actual transition time, τ_{TP}, is generally much faster. In terms of the landscape profile, the average τ_{TP} found from the mean transit time across a harmonic barrier in the large-barrier limit is [6,11]

$$\tau_{TP} \approx \frac{\ln(2e^{\gamma}\Delta G^{\ddagger}/k_B T)}{D\kappa_b/k_B T} = \frac{\ln(2e^{\gamma}\Delta G^{\ddagger}/k_B T)}{2\pi k_0 \sqrt{\kappa_b/\kappa_w}}, \quad (2)$$

where γ is Euler's constant.

Because of the extreme technical difficulty of measuring τ_{TP}, only a handful of measurements exist. A Förster resonance energy transfer (FRET) study of folding in one RNA molecule estimated τ_{TP} for folding at 240 μs, based on time-apertured photon cross correlation of the fluorescence, but was unable to estimate it for unfolding, despite the expected symmetry [5]. More recently, another FRET study measured τ_{TP} for two-state folding in proteins by analyzing the trajectories photon by photon as the proteins moved across the energy barrier [7]. The results, $\tau_{TP} \sim 2$ μs and <10 μs for two different proteins, were considerably faster than the earlier RNA study and agreed well with expectations based on the ~ 1 μs "speed limit" for protein folding [12].

Here, we demonstrate an alternate approach for determining τ_{TP} based on energy landscapes reconstructed from high-resolution single-molecule force spectroscopy. In force spectroscopy, the extension of the molecule is measured as the structure changes in response to an applied force [3]. The landscape parameters needed to calculate τ_{TP} from Eq. (2) can then be found by reconstructing the full landscape profile, either from extension trajectories at constant force [13] or force-extension curves (FECs) [14,15], or else by analyzing the distribution of unfolding forces in FECs [16,17]. We applied both methods to determine τ_{TP} for a range of different nucleic acids: DNA hairpins of varied size and sequence, five different RNA

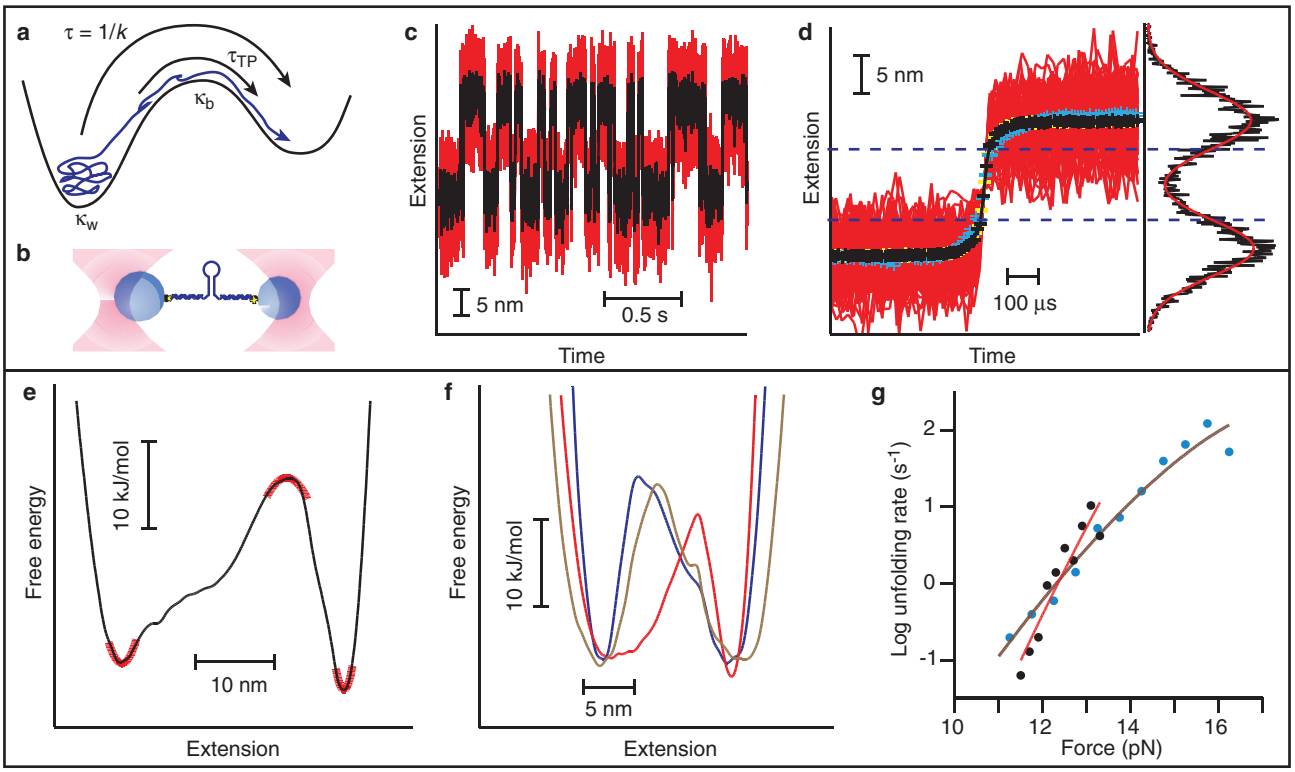

FIG. 1 (color). Extension trajectories and energy-landscape analysis of DNA hairpins. (a) Schematic free-energy profile for a folding reaction. The folding rate given by Kramers theory (k) is set primarily by the length of time spent diffusing within the potential well. The transition path time required to cross the barrier (τ_{TP}) is much shorter. κ_b: curvature of the barrier; κ_w: curvature of the well. (b) Single nucleic acid molecules attached to duplex handles are held under tension between beads in two traps. (c) The extension of hairpin 20TS06/T4 as a function of time at a constant force shows sudden changes as the hairpin folds and unfolds (red lines: data sampled at 50 kHz; black lines: filtered at 10 kHz). (d) One-ms records straddling the transitions (red lines) were aligned and averaged to reduce Brownian noise. The averages of 2529 unfolding (black line) and refolding (yellow line, time-reversed) transitions overlap with each other and with the instrument response signal from fast (< 1 μs) motions of the traps (cyan line), indicating that the apparent transition time of ~ 50 μs between the inflection points of the extension probability distributions (dashed blue lines) is instrument-limited. (e) The deconvolved landscape profile of hairpin 30R50/T4 (black line) allows the barrier and well curvatures to be measured (red curves: quadratic fits), as well as the barrier heights, thereby determining D and τ_{TP}. (f) Examples of deconvolved landscape profiles for hairpins 20TS06/T4 (blue line), 20TS10/T4 (brown line), and 20TS18/T4 (red line). (g) Fitting the force-dependent unfolding rates for 30R50/T4 (black circles) and 20TS06/T4 (cyan circles) to Equation (S2) (red and brown lines, respectively) reveals that the hairpins have very different unfolding rates at zero force.

pseudoknots, and a riboswitch aptamer. These choices allowed us to investigate the effects of different properties on τ_{TP}, such as molecule size, secondary versus tertiary structure, and ligand-induced interactions. In each case, the nucleic acids being studied were attached to kilobase-long double-stranded "handles" held by beads in a high-resolution dual-beam optical trap [18] [Fig. 1(b)].

We first looked at four DNA hairpins (30R50/T4, 20TS06/T4, 20TS10/T4, 20TS18/T4) whose folding under tension as cooperative two-state systems has been extensively characterized [13,15,19]. To see if the finite transition time between the folded and unfolded states could be observed directly, the extension of a hairpin held under constant tension was measured at 50 kHz bandwidth [Fig. 1(c)]. The effects of Brownian noise, which might obscure the transition, were reduced by aligning each 1-ms segment containing a transition of a given type (folding or unfolding) on the center of the transition [Fig. 1(d), red lines] and averaging all the segments [20]. The average of 2529 unfolding transitions [Fig. 1(d), black line] is the same as the time-reversed average of 2529 folding transitions [Fig. 1(d), yellow line], indicating that the transition is symmetric. The total time for the transition was then estimated by measuring the time required to move between the inflection points of the Gaussian extension distributions of the two states [Fig. 1(d), dashed blue lines]. The result from averaging 14 766 transitions was 49 ± 3 μs, 5 times faster than the transition time found for RNA using a FRET [5].

Such measurements do not truly give the trajectory of the hairpin during the transitions, however, because the optical trap filters the hairpin trajectory owing to the finite time required for the beads and handles to respond to motions of the hairpin [20]. To estimate the time resolution of the trap, we measured the "transition time" needed to

move beads tethered by double-stranded DNA without any hairpin through a distance similar to the extension change of the hairpin [Fig. 1(d), cyan line]. The transition time for this reference construct was identical to the transition time measured with the hairpin, 50 ± 5 μs, indicating that τ_{TP} for the hairpin must be considerably smaller. Hence, the 50-μs transition time obtained directly from the trajectories represents an upper bound.

To obtain a better estimate of τ_{TP}, we turned to the folding energy-landscape profiles reconstructed from an inverse Boltzmann transform of the extension probability distribution, removing the resolution-limiting instrumental compliance effects by deconvolution [13]. Measuring the barrier height and potential well curvatures from the energy profiles [Figs. 1(e) and 1(f)] and using the rates measured directly from the trajectories, we found D and hence τ_{TP} for each hairpin from Eqs. (1) and (2) (Table I). D is similar for all hairpins and lies within the range 10^{-11}–10^{-13} m^2/s inferred from measurements on single-stranded DNA and DNA hairpins [21–23], confirming the validity of the energy-landscape analysis approach. The values for τ_{TP}, ~6–30 μs, are all lower than the upper bound established by direct examination of the folding trajectories. They are similar in magnitude to τ_{TP} for small proteins [7] but somewhat higher, likely due to the different folding mechanism in nucleic acids compared to proteins [4]. For each hairpin, τ_{TP} for folding and unfolding agreed well (e.g., $\tau_{TP} = 30 \pm 6$ μs for folding 30R50/T4, $\tau_{TP} = 33 \pm 8$ μs for unfolding), as expected; hence, only the averaged value was reported in Table I.

It can be technically very challenging to reconstruct the full energy-landscape profile. However, D and τ_{TP} can still be estimated from more limited knowledge of key parameters describing the landscape by making some reasonable assumptions about the shape of the profile. For example, assuming a linear-cubic potential profile [16] (locally quadratic in the well and the barrier), D is given in terms of $\Delta G^{\ddagger}$, k_{off} (the unfolding rate at zero force), and $\Delta x^{\ddagger}$ (the distance to the barrier from the folded state) by

$$D \approx \frac{k_{off}(\Delta x^{\ddagger})^2}{\Delta G^{\ddagger}/k_B T} \exp\left(\frac{\Delta G^{\ddagger}}{k_B T}\right), \quad (3)$$

whereas τ_{TP} can be estimated from Eq. (2), assuming that $\kappa_w \sim \kappa_b$ (as is often done [6,11]). The three parameters needed for these calculations can be found for a linear-cubic profile by analyzing the distribution of unfolding forces or kinetics in FECs [16,17] [see Equations (S1) and (S2) in the Supplemental Material [24]].

To confirm that this indirect landscape analysis gives results consistent with the analysis of the full landscape profiles, 2048 FECs were measured for hairpin 30R50/T4 and 2966 FECs for hairpin 20TS06/T4. The landscape parameters obtained from fitting the force-dependent unfolding rates [Fig. 1(g), black: 30R50/T4; cyan: 20TS06/T4] to Equation (S2) and the distribution of unfolding forces to Equation (S1) (Table S1) yielded $D = 4 \times 10^{-13\pm1}$ m^2/s and $2 \times 10^{-12\pm1}$ m^2/s for hairpins 30R50/T4 and 20TS06/T4, respectively. The uncertainty is larger than when directly analyzing the full profile, but these values nevertheless agree well with the values listed in Table I. Equation (2) yielded $\tau_{TP} = 2 \times 10^{1\pm1}$ μs and $1 \times 10^{0\pm1}$ μs for hairpins 30R50/T4 and 20TS06/T4, respectively. Again, these values agree well (within error) with those listed in Table I, indicating that the two methods indeed give consistent results.

Hairpins contain only secondary structure. To investigate how tertiary structure affects D and τ_{TP}, we also studied RNA pseudoknots, which consist of two intercalated stem-loop structures [25]. Five different pseudoknots were measured, from the mouse mammary tumor virus (MMTV), the pea-enation mosaic virus-1 (PEMV1), the sugarcane yellow leaf virus (ScYLV) and its C27A mutant, and the bacteriophage T2 gene 32 (PT2G32). In each case, the full free-energy profile could not be obtained from constant-force measurements, but the key parameters needed to estimate D and τ_{TP} could still be found from FECs, as for the DNA hairpins. 300–600 FECs were measured for each of the pseudoknots. The landscape parameters obtained from fitting the distribution of unfolding forces to Equation (S1), as illustrated for representative distributions [Figs. 2(a)–2(c)], and also from fitting the complementary force-dependent lifetimes derived from these histograms [17], are listed in Table S1. The resulting diffusion constants and transition times (Table I) are more variable than for the hairpins, owing to larger uncertainties. However, averaging the values over all the pseudoknots (which have identical topologies and very similar sizes, 30–34 nucleotides) yields $\tau_{TP} = 1 \times 10^{1\pm0.7}$ μs, similar

TABLE I. Diffusion constants and transition path times from energy-landscape analysis. For the hairpins, D and τ_{TP} were calculated for folding and unfolding separately, to ascertain that they were symmetric with respect to the transition direction, then averaged. Uncertainties represent standard error on the mean.

Molecule	D (m^2/s)	τ_{TP} (μs)
DNA hairpins		
30R50/T4	$4.6 \pm 0.5 \times 10^{-13}$	31 ± 5
20TS06/T4	$5 \pm 3 \times 10^{-13}$	26 ± 9
20TS10/T4	$1 \times 10^{-13\pm0.4}$	$1.6 \times 10^{1\pm0.4}$
20TS18/T4	$2 \times 10^{-13\pm0.4}$	$6 \times 10^{0\pm0.4}$
Pseudoknots		
MMTV	$4 \times 10^{-16\pm1}$	$5 \times 10^{2\pm1}$
PEMV1	$6 \times 10^{-16\pm1}$	$3 \times 10^{2\pm1}$
ScYLV	$6 \times 10^{-14\pm1}$	$3 \times 10^{0\pm1}$
ScYLV C27A	$8 \times 10^{-15\pm1}$	$2 \times 10^{1\pm1}$
PT2G32	$1 \times 10^{-12\pm2}$	$5 \times 10^{-2\pm2}$
add riboswitch		
Without adenine	$2 \times 10^{-13\pm0.3}$	$5 \times 10^{0\pm0.3}$
With adenine	$2 \times 10^{-14\pm1}$	$6 \times 10^{1\pm1}$

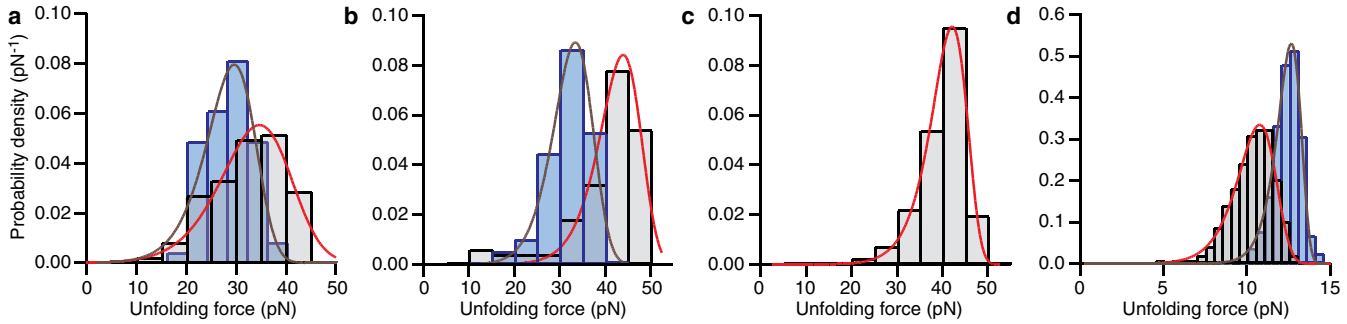

FIG. 2 (color online). Unfolding force distributions for pseudoknots and riboswitches. D and τ_{TP} were determined from the key landscape parameters obtained by fitting the unfolding force distributions from FECs to Equation (S1). (a) MMTV (blue histograms, at lower force) and PEMV1 (grey histograms, at higher force) pseudoknots. (b) ScYLV (grey histograms, at higher force) and C27A mutant (blue histograms, at lower force) pseudoknots. (c) PT2G32 pseudoknot. (d) The *add* adenine riboswitch with (blue histograms, at higher force) and without (grey histograms, at lower force) a ligand bound.

to the hairpins, and $D = 1 \times 10^{-14\pm0.7}$ m^2/s, slightly lower than for the hairpins.

To probe effects arising from different fold topologies and different tertiary interactions, we also investigated τ_{TP} for another class of RNA: the aptamer domain from a bacterial riboswitch. Riboswitch aptamers bind ligands that can induce structural changes and thereby alter the energy barrier height and unfolding rate [18,26]. Unfolding force distributions from FECs of the *add* adenine riboswitch aptamer were analyzed as for the pseudoknots [Fig. 2(d)], based on 5200 FECs measured without the adenine ligand bound and 3000 with the ligand bound. The fit results (Table S1) yielded values for D and τ_{TP} that are similar (within error) to those found for the hairpins and the pseudoknots (Table I). They are also the same (within error) whether the ligand is bound or not, even though ligand binding changes the barrier height significantly ($7k_BT$).

We note that the average transition times found for the different types of nucleic acids investigated here are roughly the same, on the order of 10 μs. This is $\sim$10 times faster than the only previous estimate of τ_{TP} for a nucleic acid [5] but comparable to τ_{TP} from measurements of small proteins [7]. Interestingly, τ_{TP} for nucleic acids is slightly higher than for proteins: the average over all the different molecules is 16 ± 8 μs, compared to $\sim$2 μs for the WW domain of the formin-binding protein [7]. This difference likely reflects the different microscopic mechanisms for folding in nucleic acids compared to proteins [4]. Nucleic acid duplex formation is often modeled as a zippering process [22,27,28], which might be expected to lead to a τ_{TP} that depends linearly on the duplex length. This is indeed what is seen comparing τ_{TP} for hairpins with different stem lengths: $\tau_{TP} = 31 \pm 5$ μs with a 30-basepair (bp) stem, whereas $\tau_{TP} = 16 \pm 4$ μs on average for 20-bp stems. The ratio of transition times, 1.9 ± 0.6, thus agrees well with the expected ratio of 1.5. The correlation of τ_{TP} with duplex length seems to extend to the RNA, as well, although the experimental uncertainty is sufficiently large that the comparison can only be made for the aptamer without a ligand bound. The transition state for aptamer unfolding involves unfolding helix P1 [18], which is only 9 bp long, and τ_{TP} for the aptamer is correspondingly shorter, at $\sim$5 μs. A plot of τ_{TP} against the length of the duplex being unfolded (Fig. 3) implies an estimate for the zippering time of $\sim$0.9 μs/bp, in reasonable agreement with previous estimates of $\sim$0.1–0.3 μs/bp from temperature-jump measurements of double helices [27] and modeling of hairpin folding rates under tension [28]. Our results disagree with a different estimate of $\sim$1–20 ns/bp from modeling hairpin folding rates under temperature jumps [29]; however, this latter estimate is unable to account for the observed τ_{TP} length dependence.

Despite the noticeable stem-length dependence of τ_{TP}, the more notable fact is that τ_{TP} is very similar for all the molecules, despite unfolding rates that differ by many orders of magnitude. The unfolding rates at zero force ranged from $\sim 10^{-3}$ s^{-1} for the MMTV pseudoknot to $\sim 10^{-21}$ s^{-1} for hairpin 30R50/T4, or 18 orders of magnitude (due largely to differences in the barrier heights). A similar effect was also seen for proteins [7], although over a

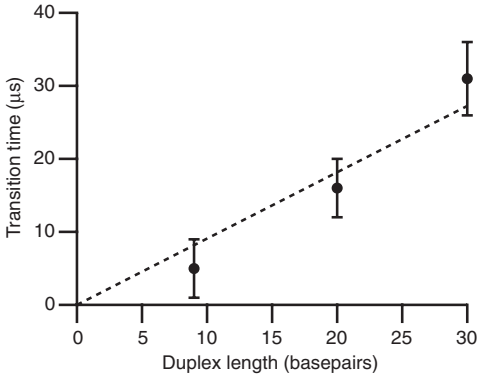

FIG. 3. Stem-length dependence of τ_{TP}. The transition time for unfolding the DNA hairpins (30- and 20-bp stems) and the riboswitch aptamer (the critical helix unfolded to reach the transition state has 9 bp) varies linearly with the length of the helix stem.

much smaller range of rates. Intuitively, this can be pictured in terms of the molecule trying to jump over the barrier with a certain initial "velocity" across the landscape: to get over a higher barrier requires a higher initial velocity (which fewer molecules have, hence lowering the total rate), but the time taken to get over the barrier is hardly changed, analogous to what happens to a projectile thrown in a parabolic trajectory. Mathematically, the effect is explained by the weak barrier-height dependence of τ_{TP} in Eq. (2).

Most remarkably, there is no significant difference in τ_{TP} for molecules with very different topologies, despite the fact that folding mechanisms are believed to be determined primarily by the topology of the native fold [30]. Single stem loops (hairpins), intercalated stem loops (pseudoknots), and triple-helix junctions (riboswitch) all produce transition times on the order of 10 μs, suggesting that τ_{TP} is relatively insensitive to the details of the folding mechanism. The values of D for the RNA structures are on average somewhat lower than for the DNA hairpins, $2 \times 10^{-14\pm0.6}$ vs $3 \times 10^{-13\pm0.2}$ m^2/s. Since D is lower for a rougher landscape, this suggests that the tertiary interactions in the pseudoknots and riboswitch roughen the landscape slightly. Assuming a random roughness distribution [31], this additional roughness is approximately $2 \pm 1 k_B T$, on average. We note that using energy-landscape analysis to obtain τ_{TP} as described here does, of course, depend on the validity of Eq. (2). Although this equation is expected to be rigorous, since it is derived from the well-established Kramers theory, it has not yet been validated formally by comparing predicted τ_{TP} values to those measured directly.

This Letter provides the first experimental measurements of τ_{TP} for both secondary and tertiary structure formation in nucleic acids. A similar approach could also be applied to determine τ_{TP} via force spectroscopy of protein folding. By determining the time required for structural transitions to take place in molecules of different size and topology, these measurements open a new window on the microscopic events occurring during biomolecular folding.

This work was supported by the National Institute for Nanotechnology, Alberta Innovates Technology Futures, Natural Sciences and Engineering Research Council, and Canadian Institutes of Health Grant Reference No. NHG 91374.

[1] J. Buchner and T. Kiefhaber, *Protein Folding Handbook* (Wiley-VCH, Weinheim, 2005).
[2] A. Borgia, P. M. Williams, and J. Clarke, Annu. Rev. Biochem. **77**, 101 (2008).
[3] M. T. Woodside, C. Garcia-Garcia, and S. M. Block, Curr. Opin. Chem. Biol. **12**, 640 (2008).
[4] D. Thirumalai and C. Hyeon, Biochemistry **44**, 4957 (2005).
[5] T.-H. Lee, L. J. Lapidus, W. Zhao, K. J. Travers, D. Herschlag, and S. Chu, Biophys. J. **92**, 3275 (2007).
[6] H. S. Chung, J. M. Louis, and W. A. Eaton, Proc. Natl. Acad. Sci. U.S.A. **106**, 11 837 (2009).
[7] H. S. Chung, K. McHale, J. M. Louis, and W. A. Eaton, Science **335**, 981 (2012).
[8] R. B. Best, Curr. Opin. Struct. Biol. **22**, 52 (2012).
[9] M. Oliveberg and P. G. Wolynes, Q. Rev. Biophys. **38**, 245 (2005).
[10] P. Hänggi, P. Talkner, and M. Borkovec, Rev. Mod. Phys. **62**, 251 (1990).
[11] G. Hummer, J. Chem. Phys. **120**, 516 (2004).
[12] J. Kubelka, J. Hofrichter, and W. A. Eaton, Curr. Opin. Struct. Biol. **14**, 76 (2004).
[13] M. T. Woodside, P. C. Anthony, W. M. Behnke-Parks, K. Larizadeh, D. Herschlag, and S. M. Block, Science **314**, 1001 (2006).
[14] G. Hummer and A. Szabo, Proc. Natl. Acad. Sci. U.S.A. **98**, 3658 (2001).
[15] A. N. Gupta, A. Vincent, K. Neupane, H. Yu, F. Wang, and M. T. Woodside, Nature Phys. **7**, 631 (2011).
[16] O. K. Dudko, G. Hummer, and A. Szabo, Phys. Rev. Lett. **96**, 108101 (2006).
[17] O. K. Dudko, G. Hummer, and A. Szabo, Proc. Natl. Acad. Sci. U.S.A. **105**, 15 755 (2008).
[18] K. Neupane, H. Yu, D. A. N. Foster, F. Wang, and M. T. Woodside, Nucleic Acids Res. **39**, 7677 (2011).
[19] M. T. Woodside, W. M. Behnke-Parks, K. Larizadeh, K. Travers, D. Herschlag, and S. M. Block, Proc. Natl. Acad. Sci. U.S.A. **103**, 6190 (2006).
[20] H. Yu, X. Liu, K. Neupane, A. N. Gupta, A. M. Brigley, A. Solanki, S. Iveta, and M. T. Woodside, Proc. Natl. Acad. Sci. U.S.A. **109**, 5283 (2012).
[21] T. Kaji, S. Ito, S. Iwai, and H. Miyasaka, J. Phys. Chem. B **113**, 13 917 (2009).
[22] A. Ansari, S. V. Kuznetsov, and Y. Shen, Proc. Natl. Acad. Sci. U.S.A. **98**, 7771 (2001).
[23] X. Wang and W. M. Nau, J. Am. Chem. Soc. **126**, 808 (2004).
[24] See Supplemental Material at http://link.aps.org/supplemental/10.1103/PhysRevLett.109.068102 for details on the materials and methods.
[25] I. Brierley, S. Pennell, and R. J. C. Gilbert, Nat. Rev. Microbiol. **5**, 598 (2007).
[26] W. J. Greenleaf, K. L. Frieda, D. A. N. Foster, M. T. Woodside, and S. M. Block, Science **319**, 630 (2008).
[27] D. Pörschke, Biophys. Chem. **2**, 97 (1974).
[28] S. Cocco, J. F. Marko, and R. Monasson, Eur. Phys. J. E **10**, 153 (2003).
[29] S. V. Kuznetsov and A. Ansari, Biophys. J. **102**, 101 (2012).
[30] D. Baker, Nature (London) **405**, 39 (2000).
[31] R. Zwanzig, Proc. Natl. Acad. Sci. U.S.A. **85**, 2029 (1988).